Synthesis of an arbitrary axial field profile by computer-generated holograms

Joseph Rosen and Amnon Yariv

Department of Applied Physics, California Institute of Technology, M.S. 128-95, Pasadena, California 91125

Received January 7, 1994

Computer-generated holograms are employed to design any desired intensity distribution along the propagation axis for a finite specified distance.

A computer-generated hologram is most commonly a transmission mask employed to construct a desired transverse image.[1] In this Letter we consider the problem of constructing a longitudinal image from a computer-generated hologram. That is, we design a mask that results in a desired arbitrary complex amplitude distribution along the propagation (z) direction at a given single transverse (x, y) point. Holographic methods for creating a longitudinal profile appear in Refs. 2–5. However, these holograms were synthesized to construct the specific case of Bessel beams only. Here we extend this concept to the general case of constructing any desired longitudinal profile by computer-generated holograms.

Rosen[6] proposed another technique to control the axial distribution, using synthetic apertures. This method was based on the Rayleigh–Sommerfeld diffraction theory and thus was applicable to the entire axial region (from the near to the far field). However, two problems arise with this method. First, the iterative algorithm for calculating the hologram sometimes diverges, and secondly, during the synthesis procedure the variable z must be changed to z^2, which causes differences between the simulated axial profile and the actual profile and leads to a degradation in the image quality. In this study these problems are eliminated.

Assume that an arbitrary transparency $g(x_1, y_1)$ is placed at the first focal plane of a lens of infinite diameter (see Fig. 1). Using the Fresnel approximation, we obtain the three-dimensional complex amplitude distribution past the lens[7]:

$$u(x,y,z) = \frac{\exp(jkz)}{j\lambda z}\int_{-\infty}^{\infty}\int_{-\infty}^{\infty} g'(x_2,y_2) \times \exp\left[-\frac{jk}{2f}({x_2}^2+{y_2}^2)\right] \times \exp\left\{j\frac{k}{2z}\left[(x-x_2)^2+(y-y_2)^2\right]\right\}\mathrm{d}x_2\mathrm{d}y_2, \quad (1)$$

where (x_2, y_2) are the coordinates of the lens's plane and $g'(x_2, y_2)$ is the field amplitude just in front of the lens, which is given by

$$g'(x_2,y_2) = \frac{\exp(jkf)}{j\lambda f}\int_{-\infty}^{\infty}\int_{-\infty}^{\infty} g(x_1,y_1) \times \exp\left\{j\frac{k}{2f}\left[(x_2-x_1)^2+(y_2-y_1)^2\right]\right\}\mathrm{d}x_1\mathrm{d}y_1. \quad (2)$$

Substituting Eq. (2) into Eq. (1), changing the order of integration, and performing the integration over x_2 and y_2, we obtain

$$u(x,y,z) = \frac{\exp[jk(z+f)]}{j\lambda f}\int_{-\infty}^{\infty}\int_{-\infty}^{\infty} g(x_1,y_1) \times \exp\left[-j\frac{k(z-f)}{2f^2}({x_1}^2+{y_1}^2) - j\frac{k}{f}(xx_1+yy_1)\right]\mathrm{d}x_1\mathrm{d}y_1. \quad (3)$$

We note that, at the second focal plane $z = f$, Eq. (3) yields the familiar Fourier integral relation between $u(x, y, z = f)$ and $g(x_1, y_1)$. Here we are interested in the field distribution along the z axis $(x, y = 0)$. Changing to polar coordinates, $(x_1, y_1) \Rightarrow (r, \theta)$, we see that Eq. (3) becomes

$$u(z) = \frac{\exp[jk(z+f]}{2j\lambda f}\int_0^{\infty} t(\rho)\exp\left[-j\frac{k(z-f)}{2f^2}\rho\right]\mathrm{d}\rho = \frac{\exp[jk(z+f)]}{2j\lambda f}\,T\left(\frac{z-f}{2\lambda f^2}\right), \quad (4)$$

where

$$t(\rho) = \int_0^{2\pi} g(\sqrt{\rho},\theta)\mathrm{d}\theta, \qquad \rho = r^2.$$

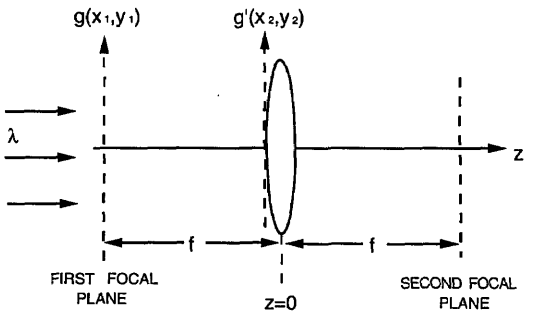

Fig. 1. Optical system used to obtain the axial Fourier transform.

0146-9592/94/110843-03$6.00/0

The significance of Eq. (4) is that, by use of a simple lens, the complex field distribution along the z axis is the one-dimensional Fourier transform of $t(\rho)$, i.e., the θ-averaged radial field profile of the original aperture at the front focal plane, with the variable $f_\rho = (z - f)/2\lambda f^2$. This spectral distribution is multiplied by the phase function $\exp[jk(z + f)]$, and its center is located at the second focal plane $z = f$. One immediate application of this Fourier relation that we demonstrate here is the tailoring of the axial intensity profile of a light beam.

The functions $t(\rho)$ and $T(f_\rho)$ are related to each other by Fourier transformation. Our goal is to find a mask $g(x_1, y_1)$, subject to some constraints, such that $|u(z)|^2$ is equal to a predefined intensity profile $I_0(z)$. To solve this problem we use the projected-onto-constraint-sets algorithm,[8] which is based on a Fourier relation among the various domains and therefore is an iterative nondiverging algorithm.[9]

In most applications it would be desirable to maximize the beam intensity along z. We thus constrain $t(\rho)$ to be a pure phase function. Because we determined that the final mask is constant along the θ axis, $g(x_1, y_1)$ is also a pure phase function. The optical system shown in Fig. 1 thus contains no absorbing elements. To design a mask $t(\rho)$ that results in a given (arbitrary) axial intensity distribution $I_0(z) = |u(z)|^2$ the projected-onto-constraint-sets algorithm may start with an arbitrary random aperture function $t_0(\rho)$. In the ith iteration of the algorithm the mask function $t_i(\rho)$ is projected onto the constraint set in the mask plane by the operator P_1, defined by $P_1[t_i(\rho)] = \exp[j\phi_i(\rho)]$, where $\phi_i(\rho)$ is the phase distribution of $t_i(\rho)$. The projected aperture is Fourier transformed to yield $T_i(f_\rho)$. This result is projected onto the constraint set in the spectral plane, where the projection is defined by

$$P_2[T_i(f_\rho)] = \begin{cases} \sqrt{I_0(f_\rho)}\exp[j\Psi_i(f_\rho)] & f_\rho \in \Delta f_\rho \\ T_i(f_\rho) & \text{otherwise} \end{cases}, \tag{5}$$

where $\Psi_i(f_\rho)$ is the phase distribution of $T_i(f_\rho)$ and Δf_ρ is some selected interval. According to Eq. (5), such a projection constrains the intensity $|u(z)|^2$ to be proportional to $I_0(z)$ along the interval $\Delta z = 2\lambda f^2 \Delta f_\rho$. The next step is to return to the mask plane by calculation of the inverse Fourier transform of $P_2[T_i(f_\rho)]$. These four operations repeat iteratively, while in every iteration we calculate the error function

$$e_i = \frac{1}{\Delta f_\rho} \int_{\Delta f_\rho} |T_i(f_\rho) - P_2[T_i(f_\rho)]|^2 \mathrm{d}f_\rho . \tag{6}$$

This expression is taken to reflect the performance of the function $t_i(\rho)$. The proof of the nondiverging property of the projected-onto-constraint-sets algorithm (i.e., $e_{i+1} \le e_i$ for all i) is given in Ref. 9. The final obtained phase function $t(\rho)$ is converted to a two-dimensional aperture function $g(x_1, y_1)$ by the relation

$$g(x_1, y_1) = g(r, \theta) = \mathrm{rect}\left(\frac{\theta}{2\pi}\right) \int_0^\infty t(\rho)\delta(\rho - r^2)\mathrm{d}\rho . \tag{7}$$

To avoid potential misalignment between the mask and the lens and to take full advantage of the holographic mask one may replace the two-element system by a single mask located, for instance, at $z = 0$. We obtain this hologram by taking $g'(x_2, y_2)$, which is the free-space propagated distribution (over f) of $g(x_1, y_1)$, and multiplying it by the transmission function of the lens. It should be mentioned, however, that, unless the constraint at the mask domain is changed, the mask this time is no longer, in general, a phase-only mask. It will thus entail some absorption and a diminution of the axial intensity, compared with the configuration employing a lens.

Two independent factors may determine the length of the axial interval over which we may specify the intensity profile. One factor is the diameter of the lens, and the other is the resolution of the mask. When the limitation is due to the mask's resolution the axial interval extends over the distance of $f + 2\lambda f^2/b^2$ from the lens, where b is the minimal ring width on the mask (we define the limit of the axial interval as the first zero of the associated sinc function). This interval starts immediately after the lens when $f < b^2/2\lambda$ or at a distance $f - 2\lambda f^2/b^2$ from the lens when $f > b^2/2\lambda$. When the system is lens-size limited and $f < b^2/2\lambda$, the longitudinal interval is determined from simple geometrical optics considerations[2] as $\Delta z = Df/d$, where D is the lens diameter and d is the mask diameter. In this study it is assumed that the system is mask-resolution limited.

As a first example, we simulate a hologram that constructs a constant intensity distribution for a specified distance along the propagation axis. Figure 2(a) shows a cross section of the phase distribution of the phase-only mask obtained from the projected-onto-constraint-sets algorithm after 400 iterations. The mask contains 128 × 128 pixels. The intensity distribution along the z axis, which was obtained by a computer simulation, is shown in Fig. 2(b). A transversal cross section of the intensity distribution over the second focal plane is depicted in

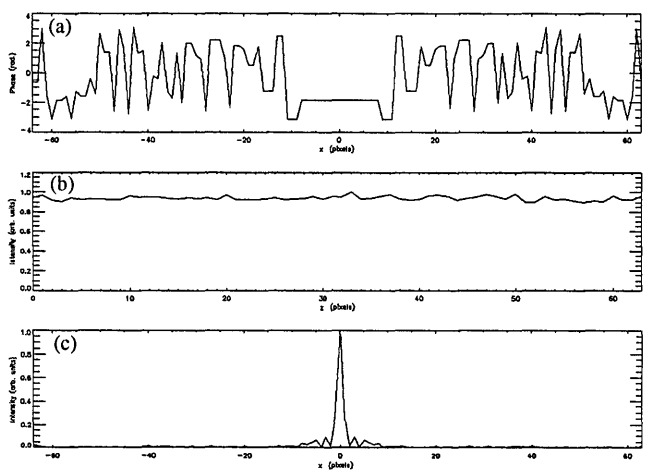

Fig. 2. (a) Cross section of the phase distribution of the hologram obtained by the projected-onto-constraint-sets algorithm. (b) Axial intensity distribution simulated by the computer. (c) Transversal intensity cross section of the beam at the second focal plane.

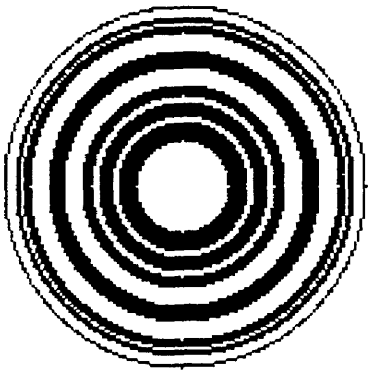

(a)

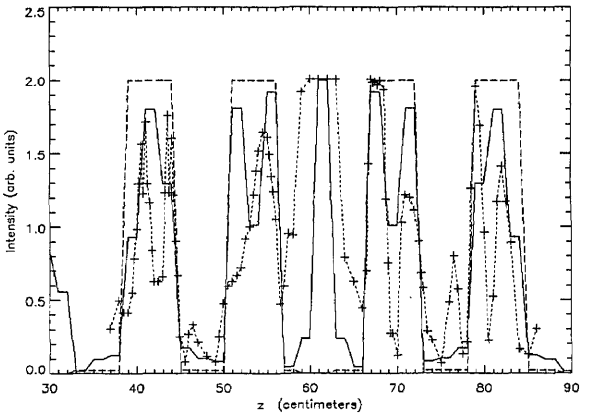

(b)

Fig. 3. (a) Hologram obtained by the direct-binary-search algorithm. (b) Axial intensity distribution obtained around the second focal length. The long-dashed curve is the desired profile, the solid curve is the simulated result, and the crosses connected by the short-dashed curve are the experimental measurements.

Fig. 2(c). We see that, at least in this plane, we have a beamlike shape, and that is the case for most of the final masks we have examined here. In the case in which, for some reason, the lateral distribution of the light is not a beamlike shape, it is possible to add constraint sets that enforce this requirement. For instance, the projection operator given in Eq. (7) of Ref. 6 may be added to the two-dimensional Fourier transform of $g(x_1, y_1)$ to produce a beamlike shape at the second focal plane.

In the laboratory we are able to produce only binary masks. This leads us to the extensive field of producing binary computer-generated holograms.[10] In our case, however, the calculations of the computer-generated holograms' values are done with one-dimensional vectors. From Ref. 10 we know that, with a binary vector, we can control, within a reasonable reconstructed error, only a limited range of the spectral plane far from the origin. Since in our example we are limited to a binary vector of 32 pixels [describing the function $t(\rho)$], a preferable algorithm (with respect to search time and final reconstruction error) is the direct binary search.[10]

In Fig. 3(a) we show the mask used in our experiment. This mask was calculated by four iterations of the direct-binary-search algorithm. The hologram was displayed on a magneto-optics spatial light modulator (128 × 128 pixels) illuminated by a plane wave in the optical system, as shown in Fig. 1 ($f = 61$ cm). The results appear in Fig. 3(b). The long-dashed curve shows the desired intensity profile $I_o(z)$, and the solid curve represents the resulting longitudinal intensity distribution simulated by the computer. The crosses connected by the short-dashed curve are the measured intensity values obtained around the second focal plane. Since the spatial light modulator is not an ideal bipolar transparency, a high intensity level is obtained at the focal region, which is truncated and not shown in this figure.

So far we have concerned ourselves solely with the axial synthesis $u(0, 0, z)$ of the beam. With this accomplished, the question of the off-axis $u(x, y, z)$ behavior of the beam is of interest. It is impossible to consider the general problem in full rigor; however, important quantitative conclusions can be drawn. We return to Eq. (3) for the three-dimensional field distribution. For $x, y \neq 0$ we need to consider the effect of the factor $\exp[-jk(xx_1 + yy_1)/f]$ in the integral. This factor causes $u(x, y, z)$ to differ substantially from $u(0, 0, z)$ once $k(x_1)_{\max}x/f \simeq \pi$. We thus expect $u(x, y, z) \simeq u(0, 0, z)$ for $x < \lambda f/2(x_1)_{\max}$, where $(x_1)_{\max}$ is the transverse dimension of the mask. In other words, we expect the axial intensity distribution to remain essentially a constant over a transverse dimension equal to the diffraction-limited spot size $\lambda f/2(x_1)_{\max}$ of the mask. The possibility of a nondiffracting beam[2–5] suggests itself immediately, as well as a nondiffracting dark hole and other forms of optical-beam sculpting.

We thank Joseph L. Horner and Jonathan Kane of Rome Laboratory, Mordechai Segev of the California Institute of Technology, and Jacob Barhen of the Jet Propulsion Laboratory for their valuable support and assistance. This research was performed in part at the Center for Space and Microelectronics Technology, Jet Propulsion Laboratory, California Institute of Technology, and was sponsored in part by NASA's office of Advanced Concepts and Technology.

References

1. W.-H. Lee, in *Progress in Optics,* E. Wolf, ed. (North-Holland, Amsterdam, 1978), Vol. XVI, Chap. 3, p. 119.
2. J. Durnin, J. J. Miceli, Jr., and J. H. Eberly, Phys. Rev. Lett. **58,** 1499 (1987).
3. A. Vasara, J. Turunen, and A. T. Friberg, J. Opt. Soc. Am. A **6,** 1748 (1989).
4. A. J. Cox and D. C. Dibble, Appl. Opt. **30,** 1330 (1991).
5. N. Davidson, A. A. Friesem, and E. Hasman, Opt. Commun. **88,** 326 (1992).
6. J. Rosen, Opt. Lett. **19,** 369 (1994).
7. J. W. Goodman, *Introduction to Fourier Optics,* 1st ed. (McGraw-Hill, New York, 1968), Chap. 4, p. 60.
8. H. Stark, ed., *Image Recovery Theory and Application,* 1st ed. (Academic, New York, 1987), Chap. 8, p. 277.
9. J. R. Fienup, Appl. Opt. **21,** 2758 (1982).
10. M. A. Seldowitz, J. P. Allebach, and D. W. Sweeney, Appl. Opt. **26,** 2788 (1987).